sensors

MDPI

Article

# Exoskeleton Hand Control by Fractional Order Models

**Mircea Ivanescu [1,*], Nirvana Popescu [2], Decebal Popescu [2], Asma Channa [2] and Marian Poboroniuc [3]**

1 Department of Mechatronics, University of Craiova, 200585 Craiova, Romania
2 Department of Computer Science, University Politehnica of Bucharest, 060042 Bucharest, Romania; nirvana.popescu@cs.pub.ro (N.P.); decebal.popescu@cs.pub.ro (D.P.); asma.channa@admin.muet.edu.pk (A.C.)
3 Department of Electrical Engineering, Technical University of Iasi, 700050 Iași, Romania; mpobor@tuiasi.ro
* Correspondence: ivanescu@robotics.ucv.ro

Received: 11 September 2019; Accepted: 20 October 2019; Published: 23 October 2019

**Abstract:** This paper deals with the fractional order control for the complex systems, hand exoskeleton and sensors, that monitor and control the human behavior. The control laws based on physical significance variables, for fractional order models, with delays or without delays, are proposed and discussed. Lyapunov techniques and the methods that derive from Yakubovici-Kalman-Popov lemma are used and the frequency criterions that ensure asymptotic stability of the closed loop system are inferred. An observer control is proposed for the complex models, exoskeleton and sensors. The asymptotic stability of the system, exoskeleton hand-observer, is studied for sector control laws. Numerical simulations for an intelligent haptic robot-glove are presented. Several examples regarding these models, with delays or without delays, by using sector control laws or an observer control, are analyzed. The experimental platform is presented.

**Keywords:** exoskeleton hand; fractional order model; control

## 1. Introduction

The IHRG is an intelligent haptic robotic glove system for the rehabilitation of patients that have a diagnosis of a cerebrovascular accident. This system is created by a thin textile in order to have a comfortable environment for grasping exercises. An exoskeleton architecture ensures the mechanical compliance of human fingers. The driving and skin sensor system is designed to determine comfortable and stable grasping function. This paper analyzes the dynamics of an exoskeleton hand using fractional order operators and proposes control solutions.

The number of applications in the system modelling, where the fractional order calculus (FOC) is used, has increased significantly in the last few decades. Many authors proved that non-integer order integrals and derivatives are suitable for analyses of the properties of various materials. Recent achievements in the interpretation of FOC operators allowed to apply FOC for processes that are better described by fractional order models (FOM) rather than integer order models (IOM). The role of these models in soft matter physics and viscoelastic behavior, in the theory of complex materials, its quality to include effects with non-conservative forces and power-law phenomena suggest to describe the complexity of human dynamics using FOM operators [1].

The idea is supported by the evidence of $s^{\beta}$ dynamics in muscles and joint tissues throughout human musculo-skeletal system [2,3]. Interaction and dependence between biological systems and associated mechanical components was analyzed in [4–6]. Fractional order models for metal polymer composite was discussed in [7]. In [8,9] viscoelastic properties for a large variety of biological entities

were studied. A class of sensors based on fractional calculus was presented in [10]. Optimal techniques using fractional calculus for sensor networks were discussed in [11]. A fractional model to capture muscular dynamics in the movement process was proposed in [12]. In [13–15] a class of neural, muscular, and vascular processes were studied to minimize sensor placement. Recently, there is a great deal of interest in so-called rehabilitation robotics, a branch of the areas of robotics and mechatronics that addresses the study of complex robotic systems aiming to restore human functions for those who suffer major trauma as a result of strokes and cerebrovascular accidents. Robotic therapy is a promising form of neurorehabilitation that can be delivered in more intensive regimens compared to conventional therapy [16]. The complexity of these systems associated with a specified class of sensors is well described by fractional order differential equations [17,18]. The methods for the analysis and design of fractional order operators can be found in [19]. Control and stability of FOM was investigated by techniques Lyapunov in [20,21]. In particular, the authors of [22,23] discuss the stability properties of solutions of nonlinear Caputo fractional differential equations. The exponential stability of nonlinear FOM using the Lyapunov method was analyzed in [24,25]. Other control problems for a class of FOMs with delay were rigorously investigated in [26,27]. Reference [28] proposed an observer for a class of linear and nonlinear FOM using Lyapunov methods. To our knowledge, this paper is the first paper to assess FOM for systems and sensors that monitor or control human behavior. The exoskeleton architecture, which ensures a mechanical compliance of human fingers, including the driving and sensor system, determines comfortable and stable grasping functions.

The dynamics of the whole system, exoskeleton hand (EXHAND), and the sensors can be accurately described by FOM operators. A class of 3D FOM bending sensors is analyzed. The control laws based on physical significance variables, for linear and delay FOM or IOM systems, are proposed and discussed. The sector control laws for linear FOM, with delays or without delays are studied. Lyapunov techniques and the methods that derive from Yakubovici-Kalman-Popov Lemma are used, and the frequency criteria that ensure asymptotic stability of the physical significance variable closed loop system are inferred. An observer control is proposed for the complex models, EXHANDs and sensors. The asymptotic stability of the whole system, the observer-system, is studied according to sector control laws. Frequency criteria and conditions for asymptotic stability are determined. Numerical simulations for the intelligent haptic robot-glove (IHRG) are presented. Several examples regarding the FOM or IOM systems, with delays or without delays, by using sector control laws or an observer control, are analyzed. The IHRG experimental platform is then discussed.

The paper is structured as follows: Section 2.1 discusses FOM sensors and FOM systems implemented in EXHAND; Section 2.2 presents the control systems; Section 3.1 analyzes IHRG numerical simulations; and Section 3.2 presents the IHRG platform. Section 4 provides concluding remarks and discussions.

## 2. Methods

### 2.1. Fractional Order Models

Notations:

1. The fractional order integral of order β is the Riemann-Liouville fractional integral:

$$I^{\beta} = \frac{1}{\Gamma(\beta)} \int_0^t f(\theta)(t-\theta)^{\beta-1} d\theta$$

2. The Caputo derivative of order $\beta$, $0 < \beta < 1$ is:

$$D^{\beta} f(t) = \frac{1}{\Gamma(\beta-1)} \int_0^t \dot{f}(\theta)(t-\theta)^{-\beta} d\theta$$

where β is the fractional order exponent and Γ(β) is the gamma (Euler's) function.

(a) 3D curvature sensors described by FOM

Bending sensors represent a class of sensors with large applications in the control of complex systems. They convert changes in bend to an electrical parameter variation. Conventional bending sensors handle cases in which bending is produced in the 2D plane. The most common are the resistive sensors, described by IOM operators of order 0. For a special class of systems, such as the hyper-redundant robots [29] where bending is produced in a 3D space (Figure 1a), a special class of bending sensors defined by FOM operators (Figure 1b) is used.

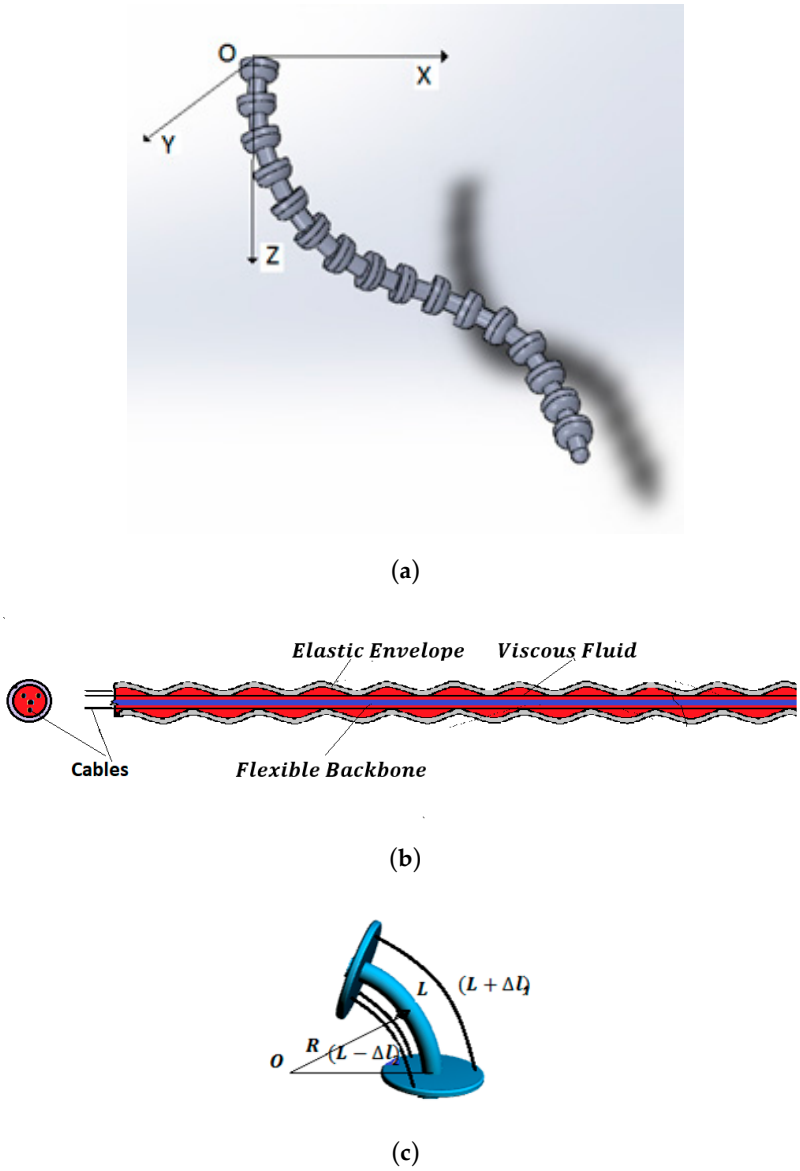


**Figure 1.** (**a**) 3D hyper-redundant robotic arm. (**b**) 3D FOM curvature sensor. (**c**) Measurement technique.

The architecture of this sensor consists of a main viscoelastic component determined by a long flexible backbone wrapped in a cylindrical elastic envelope. Three antagonist cables are implemented at the periphery of the system. In static behavior, curvature $\kappa$ is obtained by the differential measurement of the cable lengths, Figure 1c [30]:

$$\kappa = F(\Delta L_1, \Delta L_2, \ \Delta L_3) \tag{1}$$

The dynamic behavior is inferred considering constant curvature along the length. Employing the same technique as that developed in [17] yields (Figure 2):

$$\ddot{\kappa}(t) = -c_{vs} b_s D^{\beta} \kappa(t) - k_s c_s \kappa(t) + k_M \mathcal{M}(t) \tag{2}$$

where $c_{vs}$, $k_s$ are distributed viscous and elastic coefficient, assumed uniform distributed along the length, $b_s$, $c_s$ are material parameters and $\mathcal{M}$ is the moment that determines the bending. The transfer function is derived from Equation (2) as:

$$H_s(s) = \frac{\kappa(s)}{\mathcal{M}(s)} = \frac{k_M}{s^2 + c_{vs} b_s s^{\beta} + k_s c_s} \tag{3}$$

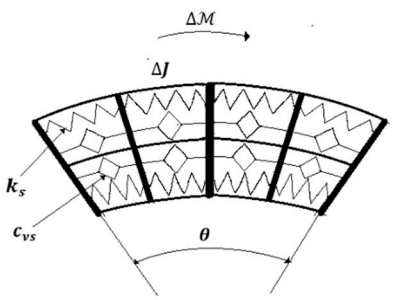


**Figure 2.** Technological equivalent model of the 3D curvature sensor.

That corresponds to an order 2 FOM operator.

(b) FOM systems

A large class of systems that monitors or controls the human behavior is well described by the FOM operators. Figure 3 shows the control system of an intelligent haptic robot-glove (IHRG) for the rehabilitation of patients that have a diagnosis of a cerebrovascular accident. The IHRG is a medical device that acts in parallel to a hand in order to compensate for lost functions [16]. The exoskeleton architecture that ensures the mechanical compliance of human fingers for the driving system determines comfortable and stable grasping functions.

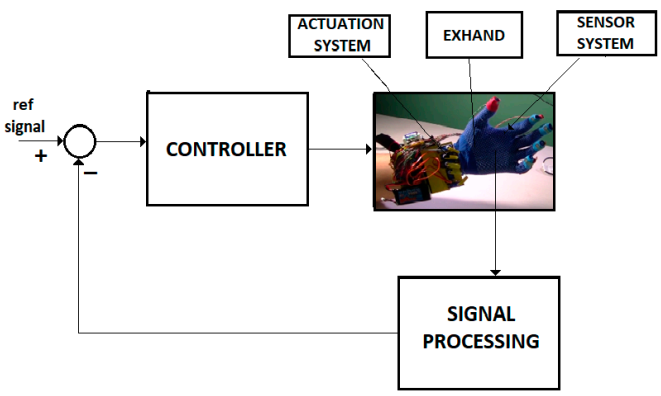


**Figure 3.** IHRG system.

The dynamics of the system (EXHAND) can be accurately described by FOM operators,

$$D^{\beta} z(t) = \boldsymbol{A}_0 z(t) + \boldsymbol{f}(z) + \boldsymbol{b} u(t), \; t \in [0, \; T] \tag{4}$$

where $z$ is the state vector $z = [z_1,\ z_2, \ldots, z_n]^T$ that defines the motion parameters, β is the fractional order exponent, and $A_0,\ b$ are $(n \times n),\ (n \times 1)$ constant matrices. In a FOM operator of EXHAND, the vector components are defined as

$$D^{\beta} z_1 = z_2,\ D^{\beta} z_2 = z_3, \ldots \tag{5}$$

The nonlinear term $f(z)$ is determined by the gravitational components and satisfies the inequality

$$\|f(z)\| < \eta \|z\| \tag{6}$$

The output of the system is generated by the bending sensors. Provided that the bending of the phalange musculoskeletal system is in 2-D plane, in this project, we used an Arduino Flex Resistive Sensor network. This sensor operates as a zeroth IOM operator,

$$y(t) = \boldsymbol{c^T z}(t) \tag{7}$$

where $c$ is a constant $(n \times 1)$ vector.

A new model can be inferred if the delay time constant, associated with the neuro-muscular system, the driving system and the processing time, is introduced,

$$D^{\beta} \boldsymbol{z}(t) = \boldsymbol{A_0 z}(t) + \boldsymbol{A_1 z}(t - \tau) + \boldsymbol{f}(z) + \boldsymbol{b} u(t),\ t \in [0,\ T] \tag{8}$$

The initial conditions are defined by

$$\boldsymbol{z}(t) = \boldsymbol{\varphi}(t),\ \ t \in [-\tau,\ 0]$$

where the function $\varphi$ is associated to initial states.

For Equations (4)–(8) we used the control system from Figure 4 with a FOM operator for the EXHAND and a IOM operator for the sensor system.

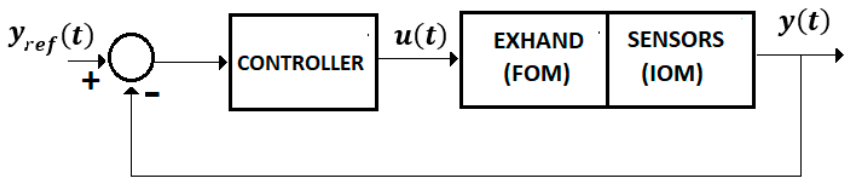


**Figure 4.** Control system.

## 2.2. Control Systems

Mathematical Preliminaries

**Lemma** [19]**.** *For any symmetric matrix* $\boldsymbol{P} \in \boldsymbol{R^{nxn}}$*, the following inequality holds:*

$$\lambda_{\min(P)} I^* \ \leq \boldsymbol{P} \ \leq \ \lambda_{\max(P)} \boldsymbol{I}^* \tag{9}$$

*where* $\lambda_{min(P)},\ \lambda_{max(P)}$ *denote the minimum and maximum eigenvalue, respectively, of matrix* $\boldsymbol{P}$ *and* $\boldsymbol{I}^*$ *is the unit matrix.*

**Theorem 1** ([21,22,24])**.** *The system* $D^{\beta} \boldsymbol{z}(t) = \boldsymbol{A z}(t),\ 0 < \beta < 1$*, is asymptotically stable if*

$$\left| Arg(eig(\boldsymbol{A})) \right| > \beta \frac{\pi}{2} \tag{10}$$

**Theorem 2** ([22–24]). *The system $D^{\beta}z(t) = f(z(t)),\ z(t_0) = z_0$ is asymptotically stable if there exists a continuously differentiable function $V(t,\ z)$ that satisfies*

$$\alpha_1\|z\|^2 \ \leq V(t,\ z(t)) \leq \ \alpha_2\|z\|^2 \tag{11}$$

$$D^{\beta}V(t,\ \boldsymbol{z}(t)) \leq \ -\alpha_3\|z\|^2 \tag{12}$$

*where $\alpha_1,\ \alpha_2,\ \alpha_3$ are positive constants,*

$$0 < \beta < 1.$$

2.2.1. Control for the EXHAND Without Delays

Consider the system from Figure 4 defined by Equations (4)–(7) without a delay time. Assume a control law.

$$u(t) = -k\Big(y(t) - y_{ref}(t)\Big) \tag{13}$$

where the control gain $k$ verifies the condition

$$k\sigma \ \leq 1 \tag{14}$$

where σ is a positive constant (for simplicity, $y_{ref}(t) = 0$).

**Remark 1.** *For the EXHAND model with the state variables defined by Equation (5) and the output vector $c = [c_1.\ c_2,\ c_3,\ c_4]^T$, the control law (Equation (10)) becomes a PD$^{\beta}$ law*

$$u(t) = -k\Big(c_1z_1 + c_2D^{\beta}z_1 + c_3z_3 + c_4D^{\beta}z_3\Big)$$

*or*

$$u(t) = -k_1z_1 - D^{\beta}z_1 - k_3z_3 - k_4D^{\beta}z_3 \tag{15}$$

*If $c$ is selected as $c = [c_1.\ 0,\ c_3,\ 0]^T$, the control becomes a PD law*

$$u(t) = -k_1z_1 - k_3\dot{z}_1 \tag{16}$$

**Control System 1.** The system (Equations (4)–(7)) with the controller defined by Equations (13) and (14) is asymptotically stable if:

The matrix $\boldsymbol{A}^* = \boldsymbol{A} - \boldsymbol{R}$ is Hurwitz stable where $\boldsymbol{R} = \boldsymbol{R}^{\boldsymbol{T}} > 0$.

$$\boldsymbol{Re}\Big(\boldsymbol{c}^{\boldsymbol{T}}(\boldsymbol{j\omega I} - (\boldsymbol{A} - \boldsymbol{R}))^{-\boldsymbol{1}}\,\boldsymbol{b}\Big) \ \geq \ -\sqrt{\sigma} \tag{17}$$

$$\varrho > \ \rho_{PR} + 2\lambda_{\max(P)}\eta \tag{18}$$

where $\varrho = \left\|\Big(q + k\sqrt{\sigma}d\Big)\Big(q + k\sqrt{\sigma}d\Big)^T\right\|$, $\rho_{PR} = 2\boldsymbol{PR}$ and $Q = qq^T$, P are solutions of the Lyapunov equation [20,29].

**Proof.** Consider the Lyapunov function

$$V(z) = \ \boldsymbol{z}^{\boldsymbol{T}}\boldsymbol{Pz} \tag{19}$$

where $\boldsymbol{P} = \boldsymbol{P^T} > 0$. The first asymptotic stability conditions (Equation (8)) are verified for $\alpha_1 = \lambda_{\min\,(P)}$, $\alpha_2 = \lambda_{\max\,(P)}$, [21] (Theorem 1), where $\lambda_{\min\,(P)}$, $\lambda_{\max\,(P)}$ denote the minimum and maximum eigenvalues of P. The fractional derivative of Equation (14) will be [22,24],

$$D^{\beta}V(z) \leq \left(D^{\beta}\boldsymbol{z^T}\right)\boldsymbol{Pz} + \boldsymbol{z^T P}\left(D^{\beta}\boldsymbol{z}\right) \tag{20}$$

By substituting Equation (4) into Equation (20), one derives

$$D^{\beta}V(z) \leq \boldsymbol{z^T}\left(\boldsymbol{A^T P} + \boldsymbol{PA}\right)\boldsymbol{z} + \boldsymbol{2z^T Pbu} + \boldsymbol{2z^T Pf} \tag{21}$$

Employing the condition (a) yields

$$D^{\beta}V(z) \leq \boldsymbol{z^T}\left((\boldsymbol{A}-\boldsymbol{R})^{\boldsymbol{T}}\boldsymbol{P} + \boldsymbol{P}(\boldsymbol{A}-\boldsymbol{R})\right)\boldsymbol{z} + \boldsymbol{2z^T Pbu} + \boldsymbol{2z^T PRz} + \boldsymbol{2z^T Pf} \tag{22}$$

Considering Equations (13) and (14), this inequality becomes

$$D^{\beta}V(z) \leq \boldsymbol{z^T}\left((\boldsymbol{A}-\boldsymbol{R})^{\boldsymbol{T}}\boldsymbol{P} + \boldsymbol{P}(\boldsymbol{A}-\boldsymbol{R})\right)\boldsymbol{z} + \boldsymbol{2z^T}\left(\boldsymbol{Pb} - \frac{\boldsymbol{1}}{\boldsymbol{2}}\boldsymbol{c}\right)u - \sigma u^2 + 2z^T\boldsymbol{PRz} + \boldsymbol{2z^T Pf} \tag{23}$$

By employing the condition (Equation (15)) and Yakubovici-Kalman-Popov (YKP) Lemma [31], results

$$\boldsymbol{z^T}\left((\boldsymbol{A}-\boldsymbol{R})^{\boldsymbol{T}}\boldsymbol{P} + \boldsymbol{P}(\boldsymbol{A}-\boldsymbol{R})\right)\boldsymbol{z} = -\boldsymbol{qq^T} \tag{24}$$

$$\boldsymbol{Pb} - \frac{\boldsymbol{1}}{\boldsymbol{2}}\boldsymbol{c} = \sqrt{\sigma}\boldsymbol{q} \tag{25}$$

Now, considering the control law (Equation (13)), it follows that

$$D^{\beta}V(\boldsymbol{z}) \leq -\boldsymbol{z^T}\left(\boldsymbol{q} + k\sqrt{\sigma}\boldsymbol{d}\right)\left(\boldsymbol{q} + k\sqrt{\sigma}\boldsymbol{d}\right)^T\boldsymbol{z} + \rho_{PR}\boldsymbol{z^T z} + 2\lambda_{\max(P)}\eta \tag{26}$$

or, by Equation (16),

$$D^{\beta}V(\boldsymbol{z}) \leq -\alpha_3\|\boldsymbol{z}\|^2 \tag{27}$$

where

$$\alpha_3 = \varrho - \rho_{PR.} \tag{28}$$

□

### 2.2.2. Control for the EXHAND with Delay

**Control System 2.** The system described by Equation (8) with the control law defined by Equation (13) is asymptotically stable if:

1. $A_0^* = (A_0 - R)$ is Hurwitz stable, where $R = R^T > 0$

$$Re\left(c^T\left(j\omega I - A_0^*\right)^{-1}b\right) \geq -\sqrt{\sigma} \tag{29}$$

$$\varrho - \left(2\eta\lambda_{\max(P_1)} + \frac{1}{2}\lambda_{\max(D)} + 2\lambda_{\max(P_1R)} + \lambda_{\max(P_2)}\right) > 0 \tag{30}$$

$$\lambda_{\min(P_2)} - \frac{1}{2}\lambda_{\max(D)} > 0 \tag{31}$$

where $Q = qq^T$, $P_1$ are solutions of the Lyapunov equations and

$$\varrho = \left\|\left(q + k\sqrt{\sigma}c_1\right)\left(q + k\sqrt{\sigma}c_1\right)^T\right\|$$

$$D = \left(A_1^T P_1 + P_1 A_1\right)$$

**Proof.** Consider the following Lyapunov function:

$$V(z(t)) = I^{1-\beta}\left(z^T(t)\boldsymbol{P_1}z(t)\right) + \int_{t-\tau}^{t} z^T(\theta)\boldsymbol{P_2}z(\theta)d\theta \tag{32}$$

where $\boldsymbol{P_1}$, $\boldsymbol{P_2}$ are $(n \times n)$ are positive definite and symmetrical matrices, $\boldsymbol{P_1} > 0$, $\boldsymbol{P_2} > 0$, $\boldsymbol{P_1^T} = \boldsymbol{P_1}$, $\boldsymbol{P_2^T} = \boldsymbol{P_2}$. $V(z)$ satisfies the condition (Equation (11)) of Theorem 2.

$$V(z) \geq \lambda_{\min(P_1)}\left\|z(t)\right\|^2 \tag{33}$$

$$V(z) \leq \lambda_{\max(P_1)}\left\|z(t)\right\|^2 + \lambda_{\max(P_2)}\int_{t-\tau}^{t}\left\|z(\theta)\right\|^2 d\theta \leq M\left\|z(t)\right\|^2 \tag{34}$$

The derivative $D^\beta V(z)$ is computed from:

$$D^\beta V(z) = I^{1-\beta}\dot{V}(z) \tag{35}$$

where $I^{1-\beta}$ is the Riemann-Liouville fractional integral of the order $(1-\beta)$. The derivative $\dot{V}(z)$ is evaluated from Equation (32)

$$\dot{V}(z) = D^\beta(\left(z^T(t)\boldsymbol{P_1}z(t)\right) + \frac{d}{dt}\int_{t-\tau}^{t} z^T(\theta)\boldsymbol{P_2}z(\theta)d\theta \tag{36}$$

which leads to the inequality

$$\dot{V}(z) \leq (D^\beta z^T(t))\boldsymbol{P_1}z(t) + z^T(t)\boldsymbol{P_1}\left(D^\beta z(t)\right) + z^T(t)\boldsymbol{P_2}z(t) - z^T(t-\tau)\boldsymbol{P_2}z(t-\tau) \tag{37}$$

By evaluating Equation (37) along of solutions of Equation (8) it turns out that

$$\begin{aligned}\dot{V}(z) \leq z^T(t)\left(\boldsymbol{A_0^{*T}P_1} + \boldsymbol{P_1A_0^*}\right)z(t) + z^T(t)\left(\boldsymbol{A_1^TP_1} + \boldsymbol{P_1A_1}\right)z(t-\tau) + \ \boldsymbol{2}z^T(t)\boldsymbol{P_1b}u(t) + \boldsymbol{2}z^T\boldsymbol{Pf} \\ +\boldsymbol{2}z^T(t)\boldsymbol{P_1R}z(t)) + z^T(t)\boldsymbol{P_2}z(t) - z^T(t-\tau)\boldsymbol{P_2}z(t-\tau)\end{aligned} \tag{38}$$

By applying the control law Equation (28), it yields

$$\begin{aligned}\dot{V}(z) \leq z^T(t)\left(\boldsymbol{A_0^{*T}P_1} + \boldsymbol{P_1A_0^*}\right)z(t) + 2z^T(t)(\boldsymbol{P_1b} - \tfrac{c}{2})u(t) - \sigma u^2(t) + 2z^T\boldsymbol{Pf} \\ +z^T(t)\left(\boldsymbol{A_1^TP_1} + \boldsymbol{P_1A_1}\right)z(t-\tau) + 2z^T(t)\boldsymbol{P_1R}z(t) + z^T(t)\boldsymbol{P_2}z(t) \\ -z^T(t-\tau)\boldsymbol{P_2}z(t-\tau)\end{aligned} \tag{39}$$

The following inequality will be used [23]

$$\left\|z^T(t)\boldsymbol{D}z(t-\tau)\right\| \leq \left\|z(t)\right\| \left\|\boldsymbol{D}\right\| \left\|z(t-\tau)\right\| \leq \lambda_{\max(D)}\left(\frac{\left\|z(t)\right\|^2}{2} + \frac{\left\|z(t-\tau)\right\|^2}{2}\right) \tag{40}$$

Additionally, considering the YKP Lemma as in the previous Control System, yields

$$z^T\left(\left(\boldsymbol{A^*} - \boldsymbol{R}\right)^T\boldsymbol{P}_1 + \boldsymbol{P}_1(\boldsymbol{A^*} - \boldsymbol{R})\right)z = -\boldsymbol{q}\boldsymbol{q}^T \tag{41}$$

$$\boldsymbol{P_1 b} - \frac{1}{2}\boldsymbol{c} = \sqrt{\sigma}\boldsymbol{q} \tag{42}$$

Substituting this result into Equation (39), considering the inequalities of Equations (6) and (40), one derives that

$$\begin{aligned}\dot{V}(\boldsymbol{z}) \leq \quad & -\boldsymbol{z}^T(t)\Big(\boldsymbol{q} + k\sqrt{\sigma}\boldsymbol{d}\Big)\Big(\boldsymbol{q} + k\sqrt{\sigma}\boldsymbol{d}\Big)^T\boldsymbol{z}(t) \\ & +\Big(2\eta\lambda_{\max(P_1)} + \tfrac{1}{2}\lambda_{\max(D)} + 2\lambda_{\max(P_1R)} + \lambda_{\max(P_2)}\Big)\big\|\boldsymbol{z}(t)\big\|^2 \\ & -\Big(\lambda_{\min(P_2)} - \tfrac{1}{2}\lambda_{\max(D)}\Big)\big\|\boldsymbol{z}(t-\tau)\big\|^2\end{aligned} \tag{43}$$

Employing Equations (30) and (31), yields

$$\dot{V}(\boldsymbol{z}) \leq -\Big(\varrho - \Big(2\eta\lambda_{\max(P_1)} + \frac{1}{2}\lambda_{\max(D)} + 2\lambda_{\max(P_1R)} + \lambda_{\max(P_2)}\Big)\Big)\big\|\boldsymbol{z}(t)\big\|^2 \tag{44}$$

Denoted by

$$\alpha_3 = \varrho - (2\eta\lambda_{\max(P_1)} + \frac{1}{2}\lambda_{\max(D)} + 2\lambda_{\max(P_1R)} + \lambda_{\max(P_2)}$$

and from Equation (35) results

$$D^\beta V(\boldsymbol{z}) \leq -\alpha_3 \boldsymbol{z}(t)^2. \tag{45}$$

□

2.2.3. Control System with Observer for the EXHAND with Delay

Consider the linearized model of Equation (8) rewritten as

$$D^\beta \boldsymbol{z}(t) = \boldsymbol{A_L z}(t) + \boldsymbol{A_1 z}(t-\tau) + \boldsymbol{b}u(t),\ t \in [0,\ T] \tag{46}$$

$$y(t) = \boldsymbol{c^T z}(t) \tag{47}$$

where the nonlinear term was approximated by

$$\mathrm{f(z)} \cong \left.\frac{\partial \mathrm{f(z)}}{\partial \mathrm{z}}\right|_{\mathrm{z}_0} \Delta \mathrm{z} = \left.\frac{\partial \mathrm{f(z)}}{\partial \mathrm{z}}\right|_{\mathrm{z}_0} (\mathrm{z}_1 - \mathrm{z}_0) = \left.\frac{\partial \mathrm{f(z)}}{\partial \mathrm{z}}\right|_{\mathrm{z}_{0=0}} \mathrm{z}_1 \tag{48}$$

**Remark 2.** *For the EXHAND model, the pair $(A_L,\ b)$ is controllable and the pair $(C,\ A_L)$ is observable.*

Consider the system defined by Equation (46). The following observer is proposed:

$$D^\beta \hat{\boldsymbol{z}}(t) = \boldsymbol{A_L}\hat{\boldsymbol{z}}(t) + \boldsymbol{A_1}\hat{\boldsymbol{z}}(t-\tau) + \boldsymbol{b}u(t) + \boldsymbol{L_1}(y_1(t) - \hat{y}_1(t)) + \boldsymbol{L_2}(y_2(t-\tau) - \hat{y}_2(t-\tau)) \tag{49}$$

$$\hat{\boldsymbol{z}}(t) = \hat{\boldsymbol{\varphi}}(t), t \in [-\tau, 0] \tag{50}$$

$$\hat{\boldsymbol{y}}(t) = [\hat{y}_1(t)\ \hat{y}_2(t)]^T, \quad \hat{y}_1(t) = \boldsymbol{c_1^T}\hat{\boldsymbol{z}}(t), \quad \hat{y}_2(t) = \boldsymbol{c_2^T}\hat{\boldsymbol{z}}(t-\tau) \tag{51}$$

where $\hat{z} \in R^n$ is the observer state, $\hat{y} \in R^2$ is the estimated output and $L_1, L_2$ are $(n \times 1)$ observability vectors. The observer error is

$$\Delta \boldsymbol{z}(t) = \boldsymbol{z}(t) - \hat{z}(t) \tag{52}$$

defined by the following equation:

$$D^\beta(\Delta \boldsymbol{z}(t)) = \Big(A_L - L_1 c_1^T\Big)\Delta \boldsymbol{z}(t) + \Big(\boldsymbol{A_1} - \boldsymbol{L_2 c_2^T}\Big)\Delta \boldsymbol{z}(t-\tau) \tag{53}$$

$$\Delta \boldsymbol{z}(t) = \Delta\varphi, \quad t \in [-\tau, 0] \tag{54}$$

Consider the control law

$$u(t) = u_1(t) + u_2(t) = -k_1 \boldsymbol{c}_1^T \hat{z}(t) - k_2 \boldsymbol{c}_2^T \hat{z}(t-\tau) \tag{55}$$

The global state $(\hat{z}, z - \hat{z}) = (\hat{z}, \Delta z)$ is considered for the system "EXHAND-observer".

**Control System 3.** The whole system, "EXHAND-observer", Equations (46), (47), and (49)–(51) (Figure 5) with the control law (55), is asymptotically stable if

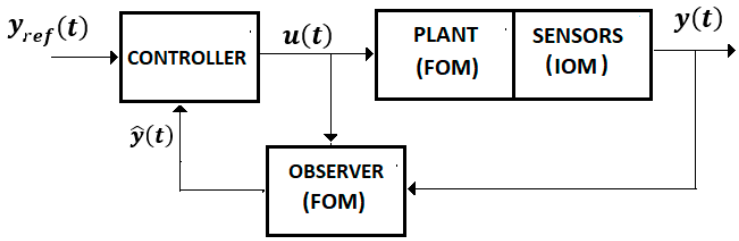


**Figure 5.** Control system with observer.

$\boldsymbol{A}_{\mathbf{L}}^* = (\boldsymbol{A}_{\mathbf{L}} - \boldsymbol{R})$ is Hurwitz stable where $\boldsymbol{R} = \boldsymbol{R}^T > 0$.

$$k_1 \sigma \leq 1, \quad \sigma > 0 \tag{56}$$

$$Re\left(\boldsymbol{c}_1^T \left(j\omega \boldsymbol{I} - \boldsymbol{A}_L^*\right)^{-1} \boldsymbol{b}\right) \geq -\sqrt{\sigma}\mathbf{q} \tag{57}$$

$$-\varrho + \lambda_{\max(D_1)} + \lambda_{\max(D_2)} + 2\lambda_{\max(P_1 R)} + \lambda_{\max(P_3)} < 0 \tag{58}$$

$$\lambda_{\max(E_1)} - \frac{1}{2}\lambda_{\max(D_1)} - \lambda_{\max(P_2)} > 0 \tag{59}$$

$$\lambda_{\max(P_2)} - \frac{1}{2}\lambda_{\max(E_2)} > 0 \tag{60}$$

$$\lambda_{\max(P_3)} - \lambda_{\max(D_2)} > 0 \tag{61}$$

where $\varrho$ is defined by Equation (50) and

$$\boldsymbol{D_2} = (\boldsymbol{L}\boldsymbol{c}_1^T)^T \boldsymbol{P_1} + \boldsymbol{P_1}\boldsymbol{L}\boldsymbol{c}_1^T; \quad \boldsymbol{D_1} = \left(\boldsymbol{A}_1^T \boldsymbol{P_1} + \boldsymbol{P_1}\boldsymbol{A_1}\right) \tag{62}$$

$$\boldsymbol{E_1} = \boldsymbol{A}_0^* - \boldsymbol{L_1}\boldsymbol{c}_1^T; \quad \boldsymbol{E_2} = \boldsymbol{A_1} - \boldsymbol{L_2}\boldsymbol{c}_2^T \tag{63}$$

**Proof.** Consider the Lyapunov function

$$V(\hat{z},\ \Delta z) = I^{1-\beta}\left(\hat{z}^T(t)\boldsymbol{P_1}\hat{z}(t) + \frac{1}{2}\Delta z^T(t)\Delta z(t)\right) + \int_{t-\tau}^{t}\left(\Delta z^T(\theta)\boldsymbol{P_2}\Delta z(\theta) + z^T(\theta)\boldsymbol{P_3}z(\theta)\right)d\theta \tag{64}$$

where $P_1,\ P_2,\ P_3$ are $(n \times n)$ are positive definite and symmetrical matrices. $V(z,\ \Delta z)$ satisfies the first condition (Equation (11)) of Theorem 2.

Applying the same procedures as in the previous control system, yields

$$\begin{aligned} \dot{V}(\hat{z},\ \Delta z) \leq\ & -\hat{z}^T(t)\left(\left(\boldsymbol{q} + k_1\sqrt{\sigma}\boldsymbol{c_1}\right)\left(\boldsymbol{q} + k_1\sqrt{\sigma}c_1\right)^T \hat{z}(t)\right. \\ & +\left(\lambda_{\max(D_1)} + \lambda_{\max(D_2)} + 2\lambda_{\max(P_1 R)} + \lambda_{\max(P_3)}\right)\left\|\hat{z}(t)\right\|^2 - \left(\lambda_{\max(E_1)} - \tfrac{1}{2}\lambda_{\max(D_1)}\right. \\ & \left.-\lambda_{\max(P_2)}\right)\left\|\Delta z(t)\right\|^2 - \left(\lambda_{\max(P_2)} - \tfrac{1}{2}\lambda_{\max(E_2)}\right)\left\|\Delta z(t-\tau)\right\|^2 \\ & -\left(\lambda_{\max(P_3)} - \lambda_{\max(D_2)}\right)\left\|\hat{z}(t-\tau)\right\|^2 \end{aligned} \tag{65}$$

By employing conditions (58)–(61) this inequality becomes

$$\dot{V}(\hat{z},\ \Delta z) \leq -\Big(\varrho - \lambda_{\max(D_1)} - \lambda_{\max(D_2)} - 2\lambda_{\max(P_1R)} - \lambda_{\max(P_3)}\Big)\left\|\hat{z}(t)\right\|^2 - (\lambda_{\max(E_1)} - \tfrac{1}{2}\lambda_{\max(D_1)} - \lambda_{\max(P_2)})\left\|\Delta z(t)\right\|^2 \tag{66}$$

and using (53) yields

$$D^{\beta}V(\hat{z},\ \Delta z) \leq -\alpha_3\left\| \begin{array}{c} \hat{z}(t) \\ \Delta z(t) \end{array} \right\|^2. \tag{67}$$

□

**Remark 3.** *The asymptotical stability conditions of Control System 2, Control System 3 are independent by the time delay $\tau$.*

## 3. Results

### *3.1. IHRG Control—Numerical Simulations*

#### 3.1.1. EXHAND with Sensors Without Delays

Consider the IHRG system of Figure 3. The exoskeleton drive system is a decoupled one, for each finger. The following parameters of the hand and exoskeleton mechanical architecture [16] will be used: the equivalent moment of inertia is $J = 0.005$ kg·m$^2$, the equivalent mass is $m = 0.015$ kg, the viscous and elastic coefficients of the equivalent Kelvin-Voigt model of the joint tissues throughout phalange musculoskeletal system and exoskeleton are [6,7] $c_v = 0.22$ Nm·s·rad$^{-1}$ $c_e = 2.8$ Nm·rad$^{-1}$, respectively, and the damping coefficient is $c_d = 7.8$ Nm·s· rad$^{-1}$.

$$J\,\ddot{\theta}(t) = -c_v\,D^{\beta}\theta(t) - c_e\,\theta(t) - c_d\,\dot{\theta}(t) + mg\sin\theta + bu(t) \tag{68}$$

$$\theta(0) = \left[\frac{\pi}{3},\ 0\right] \tag{69}$$

where the nonlinear component verifies the inequality (Equation (6)) for $\eta = 0.2$. The sensor is considered as an IOM operator and the output is defined as

$$y(t) = \boldsymbol{c^T\theta}(t) \tag{70}$$

The fractional order exponent is $\beta = \frac{1}{2}$. The FOM model (Equations (8) and (9)) is defined as

$$\theta_1 = \theta;\ D^{\frac{1}{2}}\theta_1 = \theta_2;\ D^{\frac{1}{2}}\theta_2 = \theta_3 = \dot{\theta};\ D^{\frac{1}{2}}\theta_3 = \theta_4;\ \boldsymbol{A} = \begin{bmatrix} 0\,1\,0\,0 \\ 0\,0\,1\,0 \\ 0\,0\,0\,1 \\ -0.6\ -0.1\ -7.8\ 0 \end{bmatrix};\ \boldsymbol{b} = \begin{bmatrix} 0 \\ 0 \\ 0 \\ 4.5 \end{bmatrix};\ \boldsymbol{c} = \begin{bmatrix} 1 \\ 0 \\ 1 \\ 0 \end{bmatrix}.$$

The pairs are $(\boldsymbol{A}, \boldsymbol{b})$, $(\boldsymbol{A}, \boldsymbol{c})$ controllable, respectively observable. The IOM sensor output without delays is given by (7). A control law (Equation (13)) (for $y_{ref}(t)) = 0$) with $k = 200$ is applied. This control verifies the sector constraint (Equation (11)) with $\sigma = 5 \times 10^{-3}$. The matrix R was considered as, $\boldsymbol{R} = \mathrm{diag}(3, 3, 3, 3)$ where $\boldsymbol{A_1} = \boldsymbol{A} - \boldsymbol{R}$ is Hurwitz stable. The vector $q = 0.05 \times [1111]^T$ and a matrix $P$ were inferred with $\lambda_{\max(P)} = 0.725$. The polar plot of $c^T(j\omega I - A_1)^{-1}b$ is shown in Figure 6. The closed-loop system satisfies the frequential criterion (Equation (17)), condition (18) is verified for $\left\|Q\right\| = 14.5$, $\rho = 2.17$, MATLAB/SIMULINK and techniques based on the Mittag-Leffler functions are used for the simulation [1,2]. Figure 7 shows the trajectories of fractional order variables.

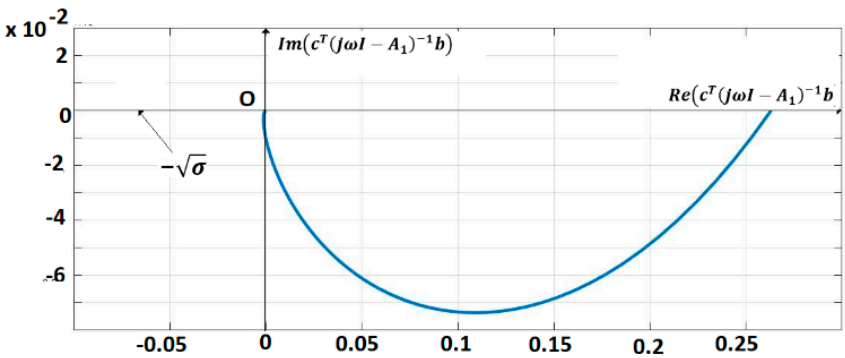


**Figure 6.** Polar plot of $c^T((j\omega I - A_1)^{-1}b$.

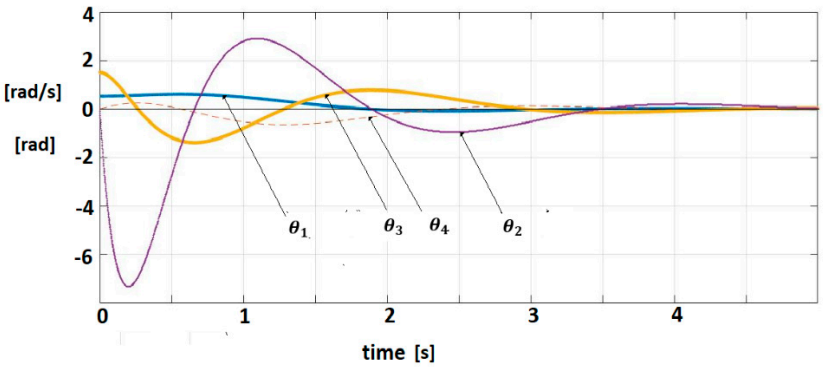


**Figure 7.** Fractional-order variable trajectories for FOM system with IOM sensor.

The steady state behavior can be analyzed by using by transfer function of Equations (65)–(67) (linearized model)

$$H_{EX}(s) = \frac{\theta(s)}{u(s)} = \frac{900}{s^2 + 44s^{\frac{1}{2}} + 1560s + 530} \tag{71}$$

The control law (Equation (13)) can be rewritten as a PD control

$$u_{PD} = -k_1 z_1 - k_3 D^{\frac{1}{2}}\left(D^{\frac{1}{2}} z_1\right) = -k_1 z_1 - k_3 \dot{z}_1 \tag{72}$$

and the controller transfer function will be

$$H_{C(PD)}(s) = k_1 + k_3\, s = \ 200(1 + s) \tag{73}$$

For the $PD^{0.5}$ control law, we have

$$H_{C(PD^{0.5})} = k_1 + k_2 s^{0.5} = 200\left(1 + s^{0.5}\right) \tag{74}$$

The steady error can be inferred from Equations (71)–(73) as [21,32,33]

$$e_{s(PD)} = e_{s(PD^{0.5})} = 0.0042$$

The behavior of the linearized model (Equation (68)) for both control laws (Equations (73) and (74)) is studied. The trajectories of angular position $\theta$ for target signal $\theta_{targ} = \frac{\pi}{6}$ are shown in Figure 8.

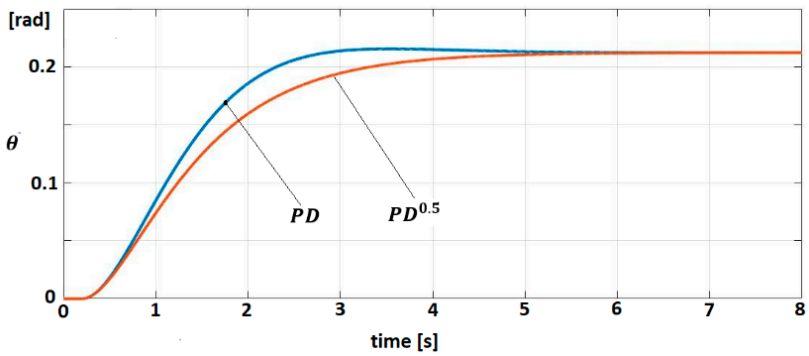


**Figure 8.** Trajectory $\theta(t)$ for PD$^{0.5}$ and PD

### 3.1.2. EXHAND with Delay

The sensor dynamics are

$$K_{s1}\, z_1(t) = y_1(t) \tag{75}$$

$$K_{s2}\, z_2(t-\tau) = y_2(t) \tag{76}$$

where $\tau \in [-0.1; 0]$. Substituting Equations (74) and (75) into (68) and using the control law (Equation (70)), yields

$$J\,\ddot{\theta}(t) = -c_v D^{\beta}\theta(t) - (c_e + K_{s1}k_1)\theta(t) - c_d\,\dot{\theta}(t) - K_{s2}k_2\,\dot{\theta}(t-\tau) + k_2 b c_2^T D^{\beta}\theta(t-\tau) + mg\sin\theta \tag{77}$$

with initial conditions

$$\theta(t) = \frac{\pi}{3},\ \dot{\theta}(t) = -1,\ t \in [-0.1; 0] \tag{78}$$

The delay component of the dynamic model is defined by $\tau = 0.1\ s$. The controller parameters are selected as $k_1 = 200,\ k_2 = 15$ that satisfy Equations (29)–(31) by employing the same parameters for $q,\ R$ as in the previous example. The evolution of the fractional order variables is shown in Figure 9.

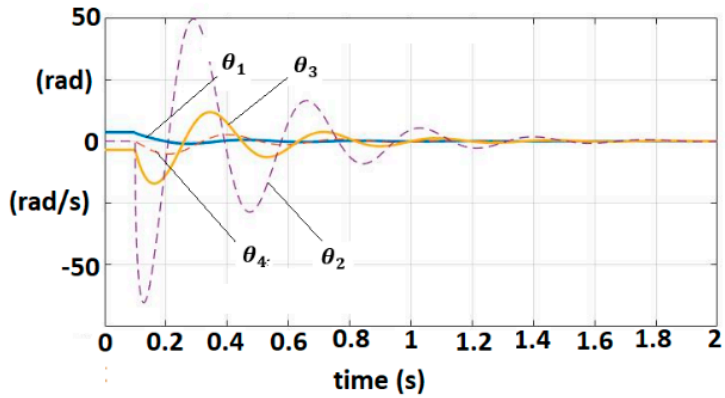


**Figure 9.** Fractional-order variable trajectories for FOM EXHAND with delay.

### 3.1.3. EXHAND with Delay and Observer

An observer (Equations (49)–(51)) with $L_1 = L_2 = [1.5\ 1.5\ 1.5\ 0]^T$ is associated to the linearized dynamic model. The matrix $R = diag(1\ 1\ 1\ 1)$ verifies the condition as $(A_{\mathrm{L}} - R)$ to be Hurwitz matrix. For $q = [0.5\ 0.5\ 0.5\ 0.5]^T$, solution of $P_1$ is obtained with $\lambda_{\max(P_1)} = 0.0085$. A control law (55) with $k_1 = 20,\ k_2 = 8.5, \sigma = 0.05$ were selected. Equations (57)–(61) are easily verified. Figure 10 shows the trajectories of physical significance variables, position and velocity, for the system and observer.

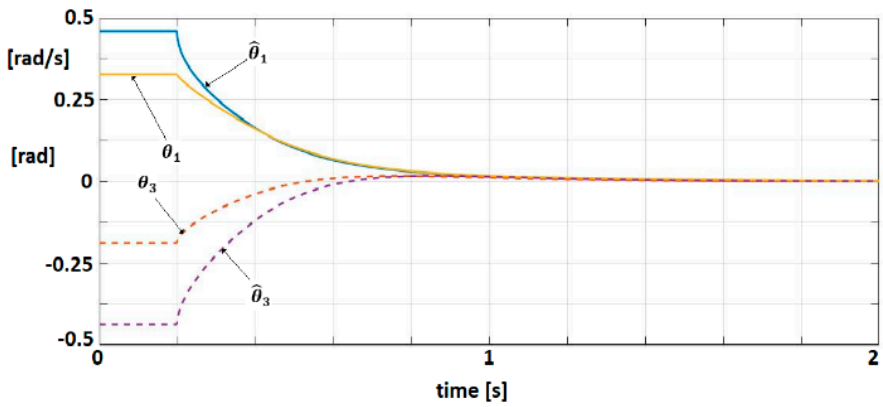


**Figure 10.** Trajectories of position and velocity for the system and observer.

### *3.2. IHRG Experimental Platform*

The IHRG is an exoskeleton that supports the human hand and hand activities by using a control architecture for dexterous grasping and manipulation. IHRG is a medical device that acts in parallel to a hand in order to compensate for lost function. It is easy to use and can be a helpful tool in the home [16,34].

The mechanical architecture consists of articulated serial elements of which design covers functional and anatomic finger phalanges. The glove is created by a thin textile that represents an infrastructure suitable for actuation wires and sensors. A distributed actuation system is used for implementing the operations of the hand. An Arduino Flex Sensor network (with zeroth order sensors) is used to control the motions. An Arduino Mega 2560 hardware platform determines the movement of the glove's actuators for exercises like opening or closing of the fingers (Figures 11 and 12).

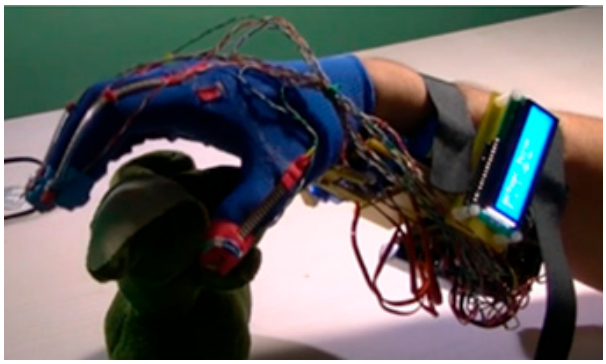

**Figure 11.** IHRG-human hand exoskeleton.

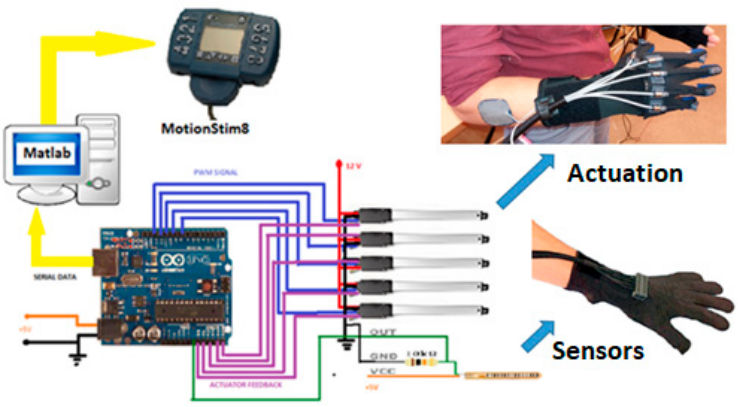


**Figure 12.** IHRG general architecture.

All the movements of the hand are controlled by the software of the hybrid IHRG system, which was developed in MATLAB and Simulink. The performance of each patient following the exercises program can be recorded by the same software. The control system of Control System 1 is implemented. In Figure 13 are shown the sensor signals during an open-close-open hand exercise.

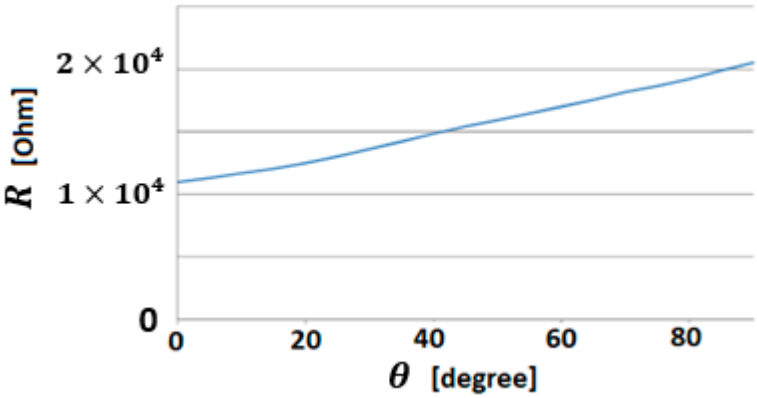


(**a**)

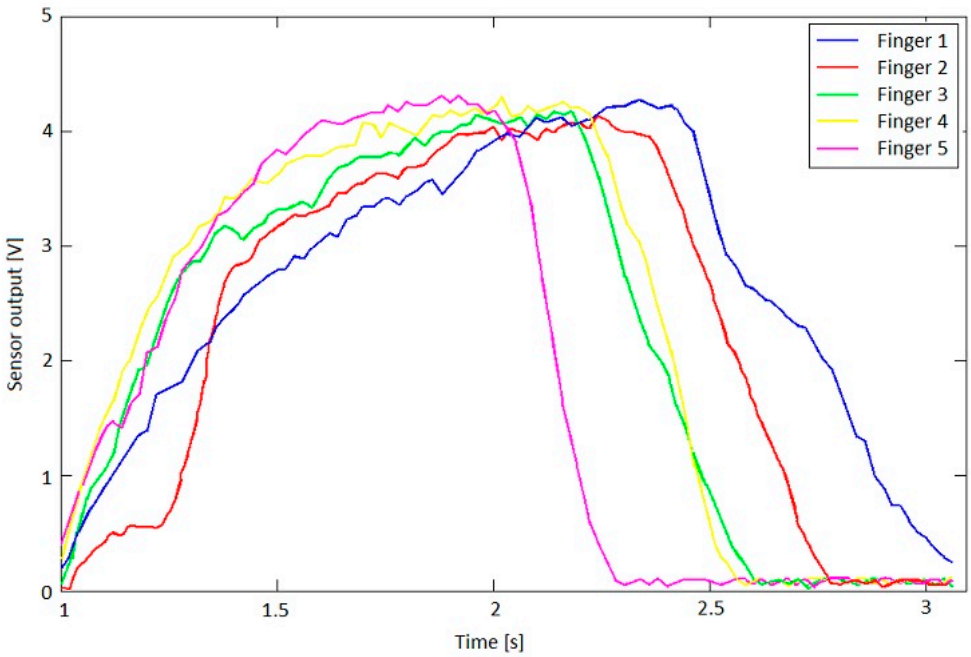


(**b**)

**Figure 13.** (**a**) Bending sensor characteristics; (**b**) Output values of the bending sensors.

## 4. Discussion

I. We designed, built, and tested an intelligent haptic robotic glove for the rehabilitation of the patients that have a diagnosis of a cerebrovascular accident. The glove is created by a thin textile in order to have a comfortable environment for the grasping exercises. This thin textile creates an infrastructure suitable for wire actuation and sensors. This exoskeleton architecture ensures the mechanical compliance of human fingers. The driving and skin sensor system is designed to determine comfortable and stable grasping function. The dynamics of the exoskeleton hand are modeled by fractional order operators. To our knowledge, this paper is the first paper in which the interaction between biological systems (human hand) and mechanical associated components (exoskeleton) is analyzed by fractional order models. These new models are used to develop a class of algorithms for

the control of the stable grasping function. The control systems are based on the physical significance variable control that are generated by sensor classes implemented in the system. These sensors are also modeled as operators with delays. The paper proposes control solutions and determines the criterions for controller parameter tuning for several classes of models. The observer techniques are also discussed and implemented. The quality and the stability of motion, are analyzed by Lyapunov methods and techniques that derive from Yakubovici-Kalman-Popov Lemma.

Despite of the model complexity, the control systems are very simple, and the controllers are easily implemented in an Arduino Mega 2560 hardware platform. There were many advantages for using this platform since this hardware board has ports for PWM signals that are useful to be sent to the actuators and ports for reading the signals coming from the bending sensors.

In order to help patients to follow an after-stoke recovery program, the system uses a set of predefined rehabilitation exercises like open the hand, close it, try to grab an object or simple wave. The system is very easy to use at home, with minimal training. The predefined rehabilitation set of exercises was created to be used.

II. The control systems discussed in the previous sections are focused on the control problems of the IHRG system, where the EXHAND model is described by FOM operators and the sensor system is based on zeroth order sensors. These control solutions can be also used for a larger class of complex systems as hyper-redundant systems, that use complex FOM sensors (Figure 14).

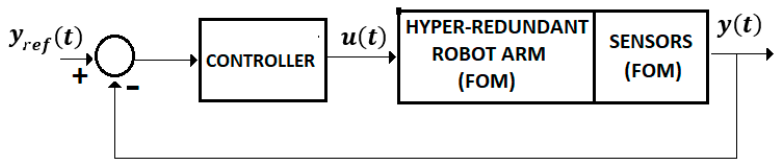


**Figure 14.** Control system with FOM sensors.

III. In addition, we consider that control systems discussed in the previous sections can be applied to a class of control problems associated to the persons with disabilities. Figure 15 presents a wheelchair control system for this class of persons. In this case, the human operator is represented by the persons with hemiparesis/hemiplegia, with motor restriction (arm or leg-emphasized hemiparesis) and with serious brain damage [35],

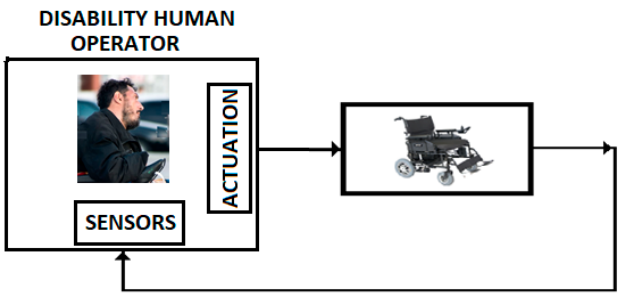


**Figure 15.** Control with disability human operator.

$$H_h(s) = k_h \frac{e^{-\tau s}}{s^{\beta}}$$

The transfer function of this human operator has a model that corresponds to a time delay fractional order model with time constant $\tau$ and fractional order $\beta$. These parameters are determined by the characteristics of the damaged brain, viscoelastic properties of the atrophied muscles, and propagation time along the nervous terminals.

We consider that these models can be studied by using the techniques developed in this paper.

**Author Contributions:** Conceptualization, M.I. and N.P.; methodology, N.P. and A.C.; software, D.P.; validation, M.I. and A.C.; formal analysis, M.P.; investigation, M.I.; resources, N.P.; data curation, D.P.; writing—A.C.; writing—review and editing, D.P.; visualization, M.P.; supervision, M.I.; project administration, N.P.; funding acquisition, N.P.

**Funding:** The authors gratefully acknowledge funding from European Union's Horizon 2020 Research and Innovation program under the Marie Sklodowska Curie grant agreement No. 813278 (A-WEAR: A network for dynamic wearable applications with privacy constraints, http://www.a-wear.eu/). This work does not represent the opinion of the European Union, and the European Union is not responsible for any use that might be made of its content

**Conflicts of Interest:** The authors declare no conflict of interest.

## References

1. Chen, Y.; Sun, R.; Zhou, A. An overview of fractional order signal processing (FOSP) techniques. In Proceedings of the ASME 2007 International Design Engineering Technical Conferences, Computers and Information in Engineering Conference, Las Vegas, NV, USA, 4–7 September 2007; pp. 1205–1222.
2. Romanovas, M.; Klingbeil, L.; Traechtler, M.; Manoli, Y. Application of Fractional Sensor Fusion Algorithms for Inertial MEMS Sensing. *Math. Model. Anal.* **2009**, *14*, 199–209. [CrossRef]
3. Debnath, K. Recent applications of fractional calculus to science and engineering. *Int. J. Math. Sci.* **2003**, *54*, 3413–3442. [CrossRef]
4. Ortigueira, M.D. A coherent approach to non-integer order derivatives. *Signal Proces. Spec. Sec. Fract. Calc. Appl. Signal Syst.* **2006**, *86*, 2505–2515. [CrossRef]
5. Sierociuk, D.; Skovranek, T.; Macias, M.; Podlubny, I.; Petras, I.; Dzielinski, A.; Ziubinski, P. Diffusion process modeling by using fractional-order models. *Appl. Math. Comput.* **2015**, *257*, 2–11. [CrossRef]
6. Tzoumas, V.; Xue, Y.; Pequito, S.; Bogdan, P.; Pappas, G.J. Selecting Sensors in Biological Fractional-Order Systems. *IEEE Trans. Control Netw. Syst.* **2017**, *5*, 134–142. [CrossRef]
7. Caponetto, R.; Graziani, S.; Pappalardo, F.L.; Sapuppo, F. Experimental Characterization of Ionic Polymer Metal Composite as a Novel Fractional Order Element. In *Advances in Mathematical Physics*; Hindawi Publishing Corporation: London, UK, 2013; p. 10.
8. Kobayashi, Y.; Watanabe, H.; Hoshi, T.; Kawamura, K.; Fujie, M.G. Viscoelastic and nonlinear liver modeling for needle insertion simulation. In *Soft Tissue Biomechanical Modeling for Computer Assisted Surgery*; Springer: Berlin/Heidelberg, Germany, 2012; pp. 41–67.
9. Wex, C.; Frolich, M.; Brandstadter, K.; Bruns, C.; Stoll, A. Experimental analysis of the mechanical behavior of the viscoelastic porcine pancreas and preliminary case study on the human pancreas. *J. Mech. Behav. Biomed. Mater.* **2015**, *41*, 199–207. [CrossRef] [PubMed]
10. Islam, T.; Shakil, S.; Lohani, B.; Mukhopadhyay, S.C. A Fractional Order Impedance Sensor for Measuring the Quality of Drinking Water. In Proceedings of the 12th International Conference on Sensor Technologies and Applications (SENSORCOMM 2018), Venice, Italy, 16–20 September 2018; pp. 25–31.
11. Dhaifallah, M.; Nassef, A.; Rezk, H.; Nisar, K.S. Optimal parameter design of fractional order control-based INC-MPPT for PV system. *Sol. Energy* **2018**, *159*, 650–664. [CrossRef]
12. Xue, Y.; Rodriguez, S.; Bogdan, P. A spatio-temporal fractal model for a cps approach to brain-machine-body interfaces. In Proceedings of the IEEE Design, Automation & Test in Europe Conference & Exhibition 2016, Dresden, Germany, 14–18 March 2016; pp. 642–647.
13. Xue, Y.; Pequito, S.; Coelho, J.M.; Bogdan, P.; Pappas, G.J. Minimum number of sensors to ensure observability of physiological systems: A case study. In Proceedings of the 54th Annual Allerton Conference on Communication, Control, and Computing, Monticello, IL, USA, 27–30 September 2016.
14. Xue, Y.; Bogdan, P. Constructing compact causal mathematical models for complex dynamics. In Proceedings of the ACM 8th International Conference on Cyber-Physical Systems, Pitsburgh, PA, USA, 18–20 April 2017; pp. 97–107.
15. Xue, Y.; Bogdan, P. Reliable multi-fractal characterization of weighted complex networks: Algorithms and implications. *Sci. Rep.* **2017**, *7*, 7487. [CrossRef] [PubMed]
16. Popescu, N.; Popescu, D.; Ivanescu, M.; Popescu, D.; Vladu, C.; Vladu, I. Force Observer-Based Control for a Rehabilitation Hand Exoskeleton System. In Proceedings of the Asian Control Conference (ASCC2013), Zurich, Switzerland, 23–26 June 2013; pp. 1–6.

17. Agila, A.; Baleanu, D. A study of multi-degree of freedom fractional order damped oscillatory system. *Upb Sci Bul.* **2018**, *80*, 52–62.
18. Vanoglio, F.; Bernocchi, P.; Mule, C.; Garofali, F.; Mora, C.; Taveggia, G.; Scalvini, S.; Luisa, A. Feasibility and efficacy of a robotic device for hand rehabilitation in hemiplegic stroke patients: A randomized pilot controlled study. *J. Clin. Rehabil.* **2016**, *31*, 351–360. [CrossRef] [PubMed]
19. Podlubny, I. Fractional Differential Equations. In *Mathematics in Science and Engineering*; Academic Press: Millbrae, CA, USA, 1999; Volume 198.
20. Diethelm, K. *The Analysis of Fractional Differential Equations*; Springer-Verlag: London, UK, 2004.
21. Petras, I. *Fractional-Order Nonlinear Systems, Modeling, Analysis and Simulation*; Springer Science & Business Media: Berlin/Heidelberg, Germany, 2011.
22. Argarwal, R.; Hristova, K.S.; O'Regan, D. Lyapunov functions and strict stability of Caputo fractional differential equations. *Adv. Differ. Equ.* **2015**, *346*, 2–20.
23. Zhao, Y.; Wang, Y.; Liu, Z. Lyapunov Function Method for Linear Fractional Order Systems. In Proceedings of the 34th Chinese Control Conference, Hangzhou, China, 28–30 July 2015; pp. 1457–1463.
24. Dadras, S.; Malek, H.; Chen, Y. A Note on the Lyapunov Stability of Fractional Order Nonlinear Systems. In Proceedings of the ASME 2017, Cleveland, OH, USA, 6–9 August 2017; pp. 123–129.
25. Al-Saggaf, U.M.; Mehedi, I.M.; Mansouri, R.; Bettayeb, M. Rotary flexible joint control by fractional order controllers. *Int. J. Control Autom. Syst.* **2017**, *15*, 2561–2569. [CrossRef]
26. Rhong, L.; Peng, X.; Zhang, B. A Reduced-Order Fault Detection Filter Design for Polytopic Uncertain Continuous-Time Markovian Jump Systems with Time-varying Delays. *Int. J. Control. Autom. Syst.* **2018**, *16*, 2021–2032. [CrossRef]
27. Khimani, D.; Patil, M. High Performance Super-twisting Control for State Delay Systems. *Int. J. Control. Autom. Syst.* **2018**, *16*, 2063–2073. [CrossRef]
28. Lee, Y.S.; Kim, D.S.; Kim, S.K. Disturbance Observer-Based Proportional-Type Position Tracking Controller for DC Motor. *Int. J. Control Autom. Syst.* **2018**, *16*, 2169–2176. [CrossRef]
29. Gravagne, L.A.; Walker, I.D. Uniform Regulation of a Multi-Section Continuum Manipulators. In Proceedings of the 2002 IEEE International Conference on Rob and Automation, Washington, DC, USA, 11–15 May 2002; pp. 1519–1525.
30. Ivanescu, M. A Decoupled Sliding Mode Control for a Continuum Arm. *Adv. Robot.* **2015**, *29*, 831–845. [CrossRef]
31. Khalil, H. *Nonlinear Systems*; Prentice Hall: Upper Saddle River, NJ, USA, 2002.
32. Heymann, N.; Podlubni, I. Physical interpretation of initial conditions for fractional differential with Riemann-Liouville fractional derivatives. *Rheol. Acta* **2014**, *7*, 45–63.
33. Tejado, I.; Abdelhamid, D.; Vinagre, B.M. *Two Strategies for Fractional Sliding Mode Control of Integer Order Systems by System Augmentation: Application to a Servomotor*; IFAC-PapersOnLine: Laxemburg, Austria, 2017; Volume 50, pp. 8103–8108.
34. Hartopanu, S.; Poboroniuc, M.; Serea, F.; Irimia, D.C.; Livint, G. New issues on FES and robotic glove device to improve the hand rehabilitation in stroke patients. In Proceedings of the 6th International Conference on Modern Power System, Cluj Napoca, Romania, 18–21 May 2015.
35. Huang, J.; Chen, Y.; Li, H.; Shi, X. Fractional Order Modeling of Human Operator Behavior with Second Order Controlled Plant and Experiment Research. *IEEE/CAA J. Autom. Sin.* **2016**, *3*, 271–280.


© 2019 by the authors. Licensee MDPI, Basel, Switzerland. This article is an open access article distributed under the terms and conditions of the Creative Commons Attribution (CC BY) license (http://creativecommons.org/licenses/by/4.0/).